CHEMISTRY

Ultrafast selective transport of alkali metal ions in metal organic frameworks with subnanometer pores

Huacheng Zhang,[1]* Jue Hou,[1] Yaoxin Hu,[1] Peiyao Wang,[2] Ranwen Ou,[1] Lei Jiang,[1,3] Jefferson Zhe Liu,[2]* Benny D. Freeman,[4] Anita J. Hill,[5] Huanting Wang[1]*

Porous membranes with ultrafast ion permeation and high ion selectivity are highly desirable for efficient mineral separation, water purification, and energy conversion, but it is still a huge challenge to efficiently separate monatomic ions of the same valence and similar sizes using synthetic membranes. We report metal organic framework (MOF) membranes, including ZIF-8 and UiO-66 membranes with uniform subnanometer pores consisting of angstrom-sized windows and nanometer-sized cavities for ultrafast selective transport of alkali metal ions. The angstrom-sized windows acted as ion selectivity filters for selection of alkali metal ions, whereas the nanometer-sized cavities functioned as ion conductive pores for ultrafast ion transport. The ZIF-8 and UiO-66 membranes showed a LiCl/RbCl selectivity of ~4.6 and ~1.8, respectively, which are much greater than the LiCl/RbCl selectivity of 0.6 to 0.8 measured in traditional porous membranes. Molecular dynamics simulations suggested that ultrafast and selective ion transport in ZIF-8 was associated with partial dehydration effects. This study reveals ultrafast and selective transport of monovalent ions in subnanometer MOF pores and opens up a new avenue to develop unique MOF platforms for efficient ion separations in the future.

INTRODUCTION

Metal ions, such as alkali metal ions of the same valence and similar subnanometer-sized ionic radii, play vital roles in life (*1*). Ultrafast selective transport of alkali metal ions across cell membranes based on sub-angstrom differences in their ionic radii is critical for cellular homeostasis and neuronal signal transduction of living systems (*2*). Biological ion channels that can intelligently regulate ion transport through cell membranes are transmembrane protein pores (*2*), consisting of subnanometer-sized ion selectivity filters and nanometer-sized cavities. Na^+ channels, integrated with selectivity filters of 3 to 5 Å in diameter and central cavities of ~12 Å in diameter (fig. S1A), exhibit a high Na^+/K^+ selectivity of 10 to 30, which is much greater than the mobility ratio of ~0.7 measured for Na^+/K^+ in water (*3*), and a selectivity sequence of $Li^+ > Na^+ > K^+ > Rb^+$ (*4*–*6*), which is opposite of the selectivity sequence of $Li^+ < Na^+ < K^+ < Rb^+$ observed in conventional synthetic porous membranes (*7*, *8*). The rate of ion transport through biological ion channels is also very high, often 10^6 ions/s or greater for a single ion channel (*2*, *5*, *9*). Rapid progress made in understanding the structures and functions of biological ion channels provides inspiration for developing porous membranes to address the most challenging issue in ion separations (*7*, *10*). For instance, Jirage and co-workers improved the ion separation efficiency of ion track–etched membranes by reducing the pore diameter to <1 nm using an electroless deposition method (*11*). Joshi *et al.* fabricated free-standing and layered graphene oxide (GO) membranes for selective transport of monatomic ions and small polyatomic ions, excluding large polyatomic ions and molecules with diameters more than 9 Å (*12*). Although these membranes had angstrom-sized pores/channels, they could only separate monatomic and small polyatomic ions over large polyatomic ions. Synthetic membranes that contain monodisperse, atomic-sized pores that can be used as ion filters to efficiently separate monatomic ions with the same valence and similar sizes (such as Li^+, Na^+, and K^+) are currently not available, even though these highly ion-selective membranes are of great interest for many applications such as in mineral extraction and ion batteries. For instance, currently, separation and purification of minerals such as lithium salts from rocks and brines involve the use of large amounts of chemicals and/or time-consuming solar ponds, which is costly and environmentally unfriendly. Therefore, the development of highly efficient lithium ion separation membranes is key to addressing this technological challenge, especially with increasing demand for energy storage materials (such as for lithium batteries) and the decline in the reserves of these resources (*13*).

Metal organic framework (MOF) membranes with a narrow distribution of pore sizes, especially in the angstrom range, are of great interest for use in separation technologies (*14*–*16*). The observation of high permeation and excellent selectivity of H_2 through $Cu_3(BTC)_2$ membranes with ~4.6 Å windows (*17*) and, more recently, through zeolitic imidazolate framework (ZIF) membranes with 3 to 5 Å windows (*18*–*22*) has led to the fabrication of a series of MOF membranes for gas separations (*23*). Some recent studies have also confirmed that MOF membranes with angstrom-sized windows, such as ZIF-8 (*24*, *25*), MIL-53 (*26*), and MOF-74 (*27*) membranes, are attractive candidates for water-related separations (*28*). Most recently, Liu *et al.* developed a UiO-66 membrane with ~6 Å windows for water desalination (*29*). However, no studies of MOF membranes for selective transport and separation of ions have been reported so far, even though the pore structures of some MOF membranes are very similar in some respects to the pore structures of biological ion channels. Specifically, the ZIF-8 [$Zn(2\text{-methylimidazolate})_2$] membrane has angstrom-sized pore windows of ~3.4 Å in diameter and nanometer-sized pore cavities of ~11.6 Å in diameter (*30*, *31*), which are similar to the angstrom-sized selectivity filters and nanometer-sized cavities of biological ion

[1]Department of Chemical Engineering, Monash University, Melbourne, Victoria 3800, Australia. [2]Department of Mechanical and Aerospace Engineering, Monash University, Melbourne, Victoria 3800, Australia. [3]Key Laboratory of Bioinspired Materials and Interfacial Science, Technical Institute of Physics and Chemistry, Chinese Academy of Sciences, Beijing 100190, People's Republic of China. [4]Department of Chemical Engineering, The University of Texas at Austin, 200 E. Dean Keeton Street, Austin, TX 78712, USA. [5]Future Industries, Commonwealth Scientific and Industrial Research Organization, Private Bag 10, Clayton South MDC, Victoria 3169, Australia. *Corresponding author. Email: huacheng.zhang@monash.edu (H.Z.); zhe.liu@monash.edu (J.Z.L.); huanting.wang@monash.edu (H.W.).

channels, respectively (fig. S1B). Thus, we hypothesize that these MOF membranes may be capable of ultrafast and selective ion transport properties.

Here, we report the experimental observation of ultrafast and selective transport of alkali metal ions through an ultrathin ZIF-8 membrane prepared by a nanoporous GO-assisted interfacial growth method on an anodic aluminum oxide (AAO) support. The resulting membrane (denoted as ZIF-8/GO/AAO membrane) can quickly and selectively transport Li^+ over other alkali metal ions based on unhydrated size exclusion, showing the following order of the ion transport rate: Li^+ (4.6) > Na^+ (3.4) > K^+ (2.1) > Rb^+ (1.0). Molecular dynamics (MD) simulations suggest that ultrafast and selective ion transport in ZIF-8 is associated with partial dehydration effects. The theoretical Li^+ mobility in ZIF-8 is faster than its transport rate in water. In contrast, synthetic nanoporous membranes have similar ion transport order to that measured in water ($Li^+ < Na^+ < K^+ < Rb^+$), indicating that the ions transport in the hydrated state in these membranes. Additional experimental results show that UiO-66 membranes with ~6.0 Å windows (larger than ZIF-8 pore windows) also have the same selectivity sequence of alkali metal ions to ZIF-8, but the ion selectivity ratios are less than those of ZIF-8. Our findings open up a new avenue to develop MOF-based membranes with diverse subnanometer pore structures and ion selectivities for efficient ion separation applications.

RESULTS

Ultrathin ZIF-8 membrane fabrication and characterization

The experiments were conducted in a typical configuration where two chambers with ionic solutions were separated by a ZIF-8/GO/AAO membrane and biased by a pair of Ag/AgCl electrodes, as shown in Fig. 1A. The ZIF-8/GO/AAO membranes used in this study are produced by a nanoporous GO-assisted interfacial growth method. Figure S2 describes the fabrication process. Hybrid two-dimensional GO nanosheets with ZIF-8 crystals were fabricated as seeds and assembled onto the AAO support by spin-coating to produce an ultrathin seeding layer (fig. S2, A and B) (*19*). Then, air plasma was used to treat the ZIF-8/GO nanosheets to make the GO nanosheets nanoporous because the nanoporous structure could facilitate fast crystal intergrowth during membrane formation (fig. S2C). Finally, the ZIF-8/GO/AAO membranes were synthesized via a counterdiffusion method at room temperature (fig. S2, D and E). During secondary growth, the nanoporous seeding layer acts as a barrier between two different synthesis solutions, self-limits crystal growth, and effectively eliminates defects during the counterdiffusion process.

Figure 1B shows scanning electron microscopy (SEM) images of ZIF-8/GO hybrid nanosheets uniformly coated on the AAO support, a cross section of the seeding layer (fig. S3), nanoporous ZIF-8/GO nanosheets obtained by air plasma treatment (Fig. 1C), a ZIF-8/GO/AAO membrane after secondary growth (Fig. 1D), and the membrane cross section (Fig. 1E). The average thickness of the ZIF-8/GO membrane on the AAO support was 446 ± 74 nm. X-ray diffraction (XRD) patterns confirmed that a highly crystalline ZIF-8 structure was formed in the ZIF-8/GO membrane after secondary growth (Fig. 1F). Gas permeation tests showed that ZIF-8/GO/AAO membranes exhibited remarkable gas selectivity (note S1 and fig. S4A), proving that the ZIF-8 membranes were of high quality with negligible defects (*19*, *32*). The N_2 adsorption-desorption isotherm profiles of ZIF-8 crystals revealed a Brunauer-Emmett-Teller (BET) surface area of 1612.7 ± 3.1 $m^2\ g^{-1}$ and a high pore volume of 0.61 $cm^3\ g^{-1}$ (fig. S4B).

Selective ion transport properties of ZIF-8 membranes

Ion transport properties of the ZIF-8/GO/AAO membranes were studied by current-voltage (*I-V*) measurements, which were performed at room temperature. Figure 2A shows typical *I-V* characteristics of a 200-nm porous AAO support in different ionic solutions (0.1 M). All tested alkali metal ion types (Li^+, Na^+, K^+, and Rb^+) exhibit a linearity in their *I-V* curves, with different transport rates for different ions and a strong dependence on their hydrated ionic diameters, based on the differential conductance values shown in fig. S5A. Because the four electrolyte solutions share the same anion (Cl^-), the differences of the ionic currents shown in Fig. 2A are mainly caused by the cations. The order of the ion transport rate through the AAO support, indicated by ion conductance, was $Li^+ < Na^+ < K^+ < Rb^+$. After the growth of the ZIF-8/GO layer onto the AAO support however, *I-V* characteristics of the ZIF-8/GO/AAO membrane (illustrated in Fig. 2B) are very different from the results shown in Fig. 2A. The order of ion transport of the ZIF-8/GO/AAO membrane was $Li^+ > Na^+ > K^+ > Rb^+$ (fig. S5B). We also systematically compared the ion conductance values of the AAO substrates before and after growth of the ZIF-8/GO layer. The LiCl conductance values (G_{LiCl}) of the ZIF-8/GO/AAO membranes were slightly higher than that of pure AAO supports, whereas the NaCl, KCl, and RbCl conductance values of the ZIF-8/GO/AAO membranes were much less than those of pure AAO supports (Fig. 2C and table S1).

As shown in fig. S3F, the interlayer spacings of the GO nanosheets within the ZIF-8 membrane varied from 5 to 30 nm, which are much larger than the angstrom-sized hydrated ionic diameters. Therefore, only the ZIF-8 with subnanometer pores is essential for the alkali metal ion selectivity of the ZIF-8/GO/AAO membrane. To further confirm that the GO nanosheets did not play an important role in ion transport properties of the ZIF-8/GO/AAO membranes, we washed the ZIF-8/GO/AAO membrane with hydrochloric acid to remove the ZIF-8 and tested the ion transport properties of the nanoporous GO/AAO membrane. Different from *I-V* curves of the ZIF-8/GO/AAO membranes shown in Fig. 2B, the GO/AAO membrane without ZIF-8 does not have alkali metal ion selectivity (fig. S6), showing an ion transport order of $Li^+ < Na^+ < K^+ < Rb^+$, which was the same as the result observed in the AAO support (Fig. 2A). Moreover, we have grown ZIF-8 inside the single-channel polyethylene terephthalate (PET) membrane without using GO nanosheets and investigated its ion transport behavior (notes S2 and S3). The result shows that such a ZIF-8/PET membrane has similar ion transport rate and ion selectivity of the ZIF-8/GO/AAO membrane (fig. S7). These results strongly suggest that GO does not play a significant role in alkali metal ion selectivity, and the unusual ion transport properties of ZIF-8/GO/AAO membranes are attributed to the subnanometer pores of ZIF-8.

Ion transport mechanism in ZIF-8 and MD simulation

To explain the observed unusual ion transport properties in ZIF-8 membranes with subnanometer pores, we suggest two different models for ion transport through AAO and ZIF-8 membranes. Ions are hydrated by water molecules in aqueous solution (*33*), and hydrated ionic diameters of alkali metal ions ($d_{H\text{-}ion}$) are ~6 to 8 Å, which is much larger than the dehydrated ionic diameters (d_{Ion}) of the ions (~1 to 3 Å) (table S2). For the AAO support, its pore diameter of ~200 nm is much larger than the hydrated ionic diameters, so the ions transported through the pores of the AAO support are hydrated, as illustrated in Fig. 2D. The order of the hydrated ionic diameter is $d_{H\text{-}Li^+}$ (7.64 Å) > $d_{H\text{-}Na^+}$ (7.16 Å) > $d_{H\text{-}K^+}$ (6.62 Å) > $d_{H\text{-}Rb^+}$ (6.58 Å) (*33*), so the conductance values of the AAO support for different ion types decrease with

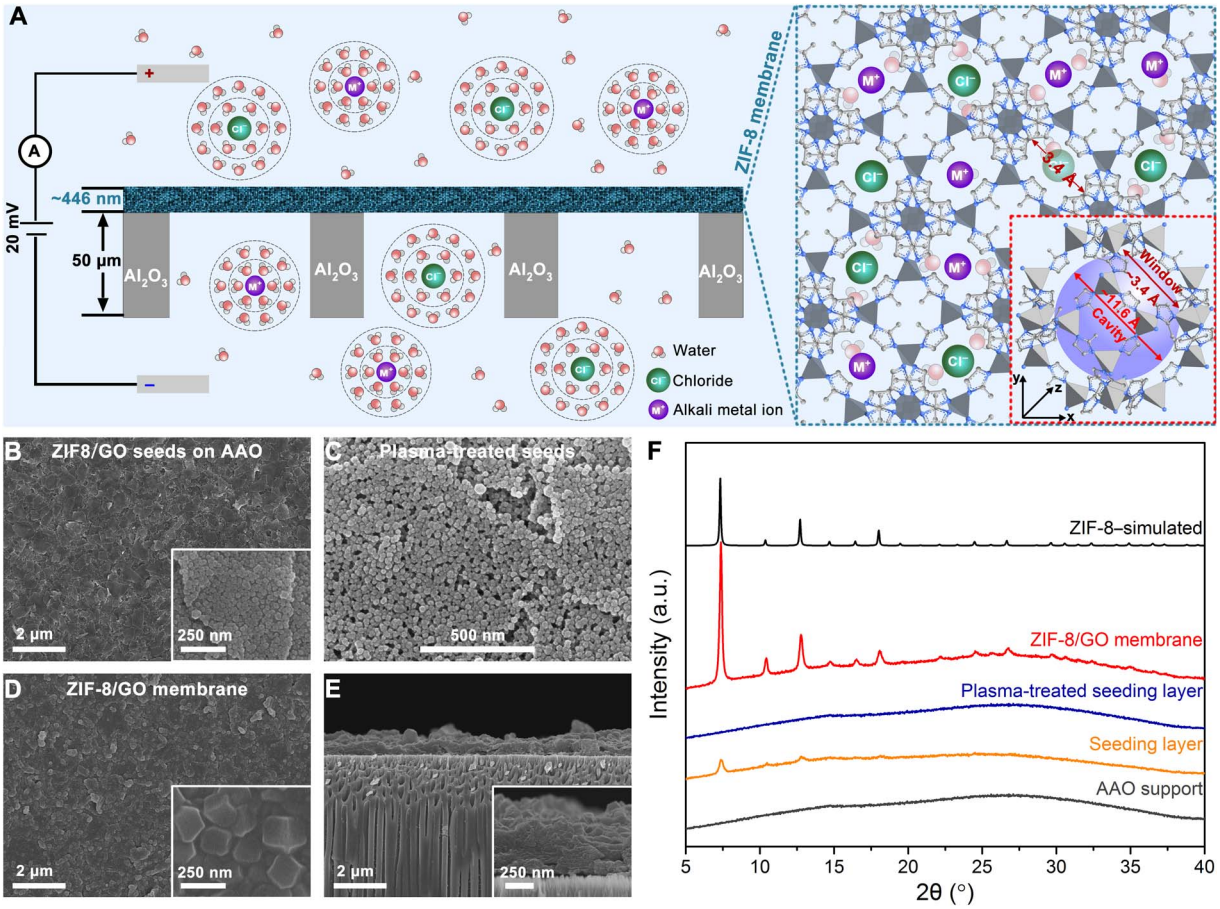

Fig. 1. Ion transport through the ZIF-8/GO/AAO membranes. (**A**) Schematic illustration of ion transport through a ZIF-8/GO/AAO membrane with ~3.4 Å pore windows for ion selectivity and ~11.6 Å pore cavities for fast ion transport (drawing not to scale). The inset indicates the crystal structure of ZIF-8. (**B**) SEM images the hybrid ZIF-8/GO nanosheet seeds coated on the AAO support. (**C**) SEM image of the plasma-treated nanoporous ZIF-8/GO seeds. (**D**) SEM images of the ZIF-8/GO/AAO membrane surface. (**E**) SEM images of the membrane cross section reveal that a ~446-nm-thick ZIF-8/GO layer is densely grown on the top of the AAO support. (**F**) XRD patterns of the AAO support, the seeding layer, the plasma-treated seeding layer, the ZIF-8/GO/AAO membrane, and simulated ZIF-8 structure. a.u., arbitrary units.

increasing hydrated ionic diameter: $G_{LiCl} < G_{NaCl} < G_{KCl} < G_{RbCl}$ (fig. S5A). However, when the pore diameter becomes less than the hydrated ionic diameter but larger than the dehydrated ionic diameter, ions should undergo a dehydration process to enter the pore (Fig. 2E), a mechanism which has been widely confirmed in biological ion channels (*2*, *9*). Dehydrated ions can be rehydrated by water molecules when they exit the pore into an aqueous solution. The ZIF-8 crystal structure contains multiple uniform ~3.4 Å windows and ~11.6 Å cavities (fig. S1B); therefore, ions passing through ZIF-8 will undergo multiple dehydration-hydration processes (fig. S8). Hence, the order of conductance values of the ZIF-8/GO/AAO membrane is as a function of the dehydrated ionic diameter. The fully dehydrated ionic diameter of alkali metal ions is in the following order: d_{Li^+} (1.20 Å) < d_{Na^+} (1.90 Å) < d_{K^+} (2.66 Å) < d_{Rb^+} (2.96 Å) (*33*), so the ZIF-8/GO/AAO membrane for different ions has opposite ion conductance values: $G_{LiCl} > G_{NaCl} > G_{KCl} > G_{RbCl}$ (fig. S5B). Given that the pore window chemistry of ZIF-8 (without specific ion-binding group) is very different from the chemistry of the selectivity filter (with specific ion-binding groups) of biological ion channels (fig. S1), the dehydration mechanism in ZIF-8 is highly likely to be different. Because of ZIF-8's unique subnanometer pore structures and many hydrophilic groups on the framework, dehydration of ions in ZIF-8 is presumably controlled by the size confinement effect and weak interactions between the confined ions and water molecules and MOF frameworks at the angstrom scale.

To support this hypothesis, MD simulations were performed to study the ion transport of LiCl and KCl in ZIF-8 and in bulk water. Figure 3A shows the molecular representation of the MD simulations. The confinement arising from the ZIF-8 crystal structure leads to the formation of separated water clusters in cavities connected via narrow windows, which is consistent with the model presented in fig. S8. The weak interactions between ions and water molecules and ZIF-8 frameworks are mainly described by van der Waals forces and Coulombic interactions (see note S4). The calculated ion mobility results are summarized in Fig. 3B and table S3 (see fig. S9 for calculated ion velocities in ZIF-8 pores). The Li^+ mobility is enhanced in ZIF-8 compared to the Li^+ mobility in water, whereas an opposite trend is observed for K^+ ions. As a result, in ZIF-8, Li^+ ions have a higher mobility than K^+ ions, which agrees with our conductance experiments. To understand this observation, Fig. 3C shows the radial distribution function of the oxygen atoms on water molecules surrounding Li^+ and K^+ ions. The water structure confined within subnanometer ZIF-8 pore is different from bulk water molecules; significant interactions between

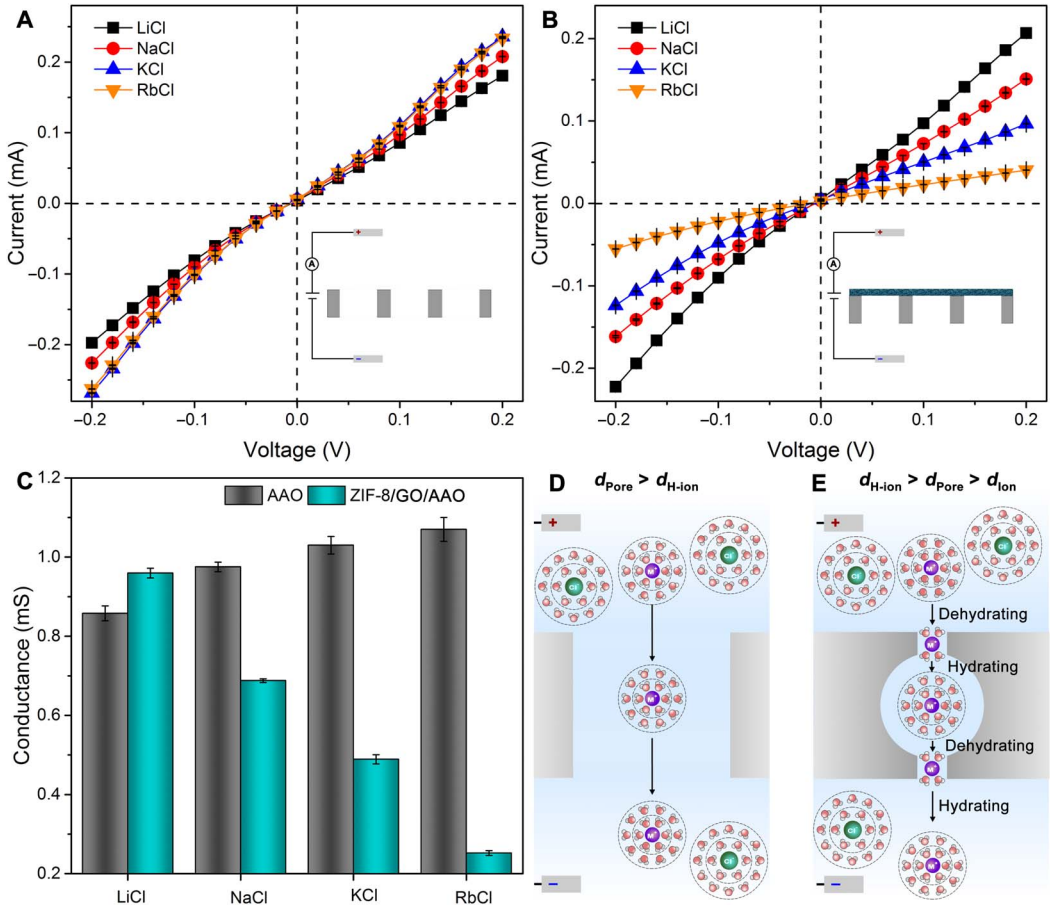

Fig. 2. Current-voltage (*I-V*) characteristics of an AAO support before and after growth of the ZIF-8/GO layer to make the ZIF-8/GO/AAO membrane. (**A**) *I-V* curves of the AAO support measured with different ions. (**B**) *I-V* curves of ZIF-8/GO/AAO membranes measured with different ions. (**C**) Ion conductance values of the AAO support with and without the ZIF-8/GO membrane. (**D**) Schematic of ion transport through a pore with a diameter much larger than the hydrated ionic diameter ($d_{Pore} >> d_{H\text{-}ion}$, such as the 200-nm porous AAO support). Ions transport in a hydrated state. (**E**) Schematic of ion transport through a simplified subnanometer ZIF-8 pore with 3.4-Å-diameter windows, which is smaller than the hydrated ionic diameters but larger than the dehydrated ionic diameters ($d_{H\text{-}ion} > d_{Window} > d_{Ion}$), and a 11.6-Å-diameter cavity, which is larger than the hydrated ionic diameters ($d_{Cavity} > d_{H\text{-}ion}$). Ions should undergo a dehydration process when they enter the window and a hydration process when they exit the window. As a result, ions passing through the subnanometer ZIF-8 pore should undergo multiple dehydration-hydration processes.

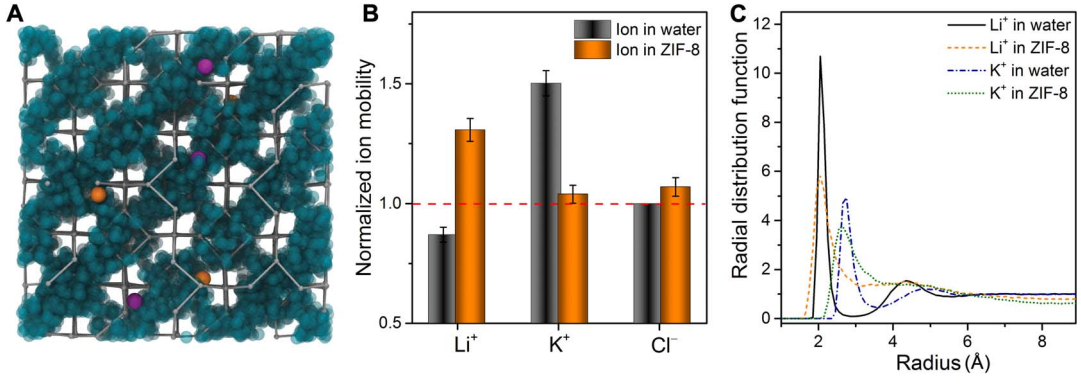

Fig. 3. MD simulations of ion transport in ZIF-8. (**A**) The simulation cartoon shows the ZIF-8 cavities filled with water molecules (green spheres), and they are connected via narrow windows. For clarity, ZIF-8 is shown as a wireframe. The apparent empty spaces are actually occupied by atoms of ZIF-8. K^+ and Cl^- ions are represented by orange and purple spheres, respectively. (**B**) The normalized mobility of K^+, Li^+, and Cl^- ions in ZIF-8 and in water. The mobility of Cl^- in 1 M aqueous solution is taken as the reference. The Li^+ mobility is enhanced in ZIF-8 compared with that in water, whereas the opposite trend is observed for K^+. Consequently, Li^+ in ZIF-8 has a higher mobility than K^+, which is consistent with experiments. (**C**) Radial distribution function of water molecules around Li^+ and K^+ in bulk solutions and in ZIF-8. Owing to the confinement effect, the water density in the first hydration shell of Li^+ is significantly reduced, and the second hydration shell nearly disappears. Similar (but less) trends can be observed for K^+. The diameter of the partly hydrated Li^+ appears to be smaller than that of the partly hydrated K^+ in ZIF-8, which might explain its higher mobility.

water molecules and ZIF-8 frameworks may compete with the water-ion interactions, resulting in partial dehydration of ions in ZIF-8. These hydration shells surrounding the ions in ZIF-8 are very different from those in the bulk solution. The reduced oxygen atom density peaks clearly suggest the partial dehydration of Li^+ and K^+ ions in ZIF-8. In ZIF-8, their second hydration shell nearly disappears (Fig. 3C). The partially dehydrated Li^+ ion apparently has a smaller effective size than K^+. Stripping water molecules from the weakened hydration shell when ions pass through the small ZIF-8 pore should cost less energy, which could explain the higher mobility of Li^+ ions in ZIF-8. Therefore, we can conclude that the ion selective mechanism in ZIF-8 pores lies in partial dehydration of ions that is controlled by the size confinement effect and weak interactions between confined ions and water molecules and MOF frameworks, mainly including van der Waals forces and Columbic interactions, and then size exclusion of the dehydrated ions.

To further examine the influence of interaction between water molecules and the ZIF-8 framework, we purposely reduced the van der Waals interaction among them by half. The calculated radial distribution function curve and mobility values of ions in ZIF-8 under reduced van der Waals force are slightly different from those calculated under the normal van der Waals (see fig. S10 and table S3). We found that the reduced van der Waals interaction cases for both Li^+ and K^+ have about 21 to 24% lower mobility than the normal cases (see table S3). This is consistent with the stronger hydration we observed in fig. S10. However, the ratio of relative mobility of Li^+ over K^+ shows only a slight change (~5%). Our results suggest that the size confinement might play a more significant role in the ion selectivity, whereas water-framework interaction apparently plays a key role in the absolute ion mobility. Note that we only explored a small region of van der Waals interactions and a fixed cage size, so this conclusion should be taken under these constraints.

DISCUSSION

Alkali metal ion selectivity and transport rate in ZIF-8

Alkali metal ion selectivities of reproduced ZIF-8/GO/AAO membranes are summarized in Fig. 4A and table S4. The ZIF-8/GO/AAO membranes do not show specific ion selectivity as high as that of biological ion channels. The Li^+/Rb^+, Li^+/K^+, and Li^+/Na^+ selectivity ratios of 4.6, 2.2, and 1.4, respectively, are the highest ever reported for synthetic membranes. It is noteworthy that the angstrom-sized pore windows of ZIF-8 are neutral and without functional groups, having no specific ion binding properties (Fig. 4B). In addition, the pore windows of ZIF-8 are flexible, without sharp sieving at 3.4 Å (*34*). Thus, the ion selectivity of the ZIF-8/GO/AAO membranes is mainly based on the sub-angstrom differences in partially dehydrated ionic diameters of alkali metal ions. Because Li^+ and Rb^+ have the largest difference in ionic diameters, the ZIF-8/GO/AAO membrane shows a higher Li^+/Rb^+ selectivity than Li^+/Na^+ or Li^+/K^+ selectivity (Fig. 4A). To confirm the stability of the ZIF-8/GO/AAO membranes, ion conductance values were cyclically tested between LiCl and RbCl solutions (0.1 M). After testing for at least three cycles, no obvious change in the conductance values at each testing state was observed (fig. S11A). Thus, the ZIF-8/GO/AAO membranes have good stability and cycling performance. The stability of the ZIF-8/GO/AAO membranes was further confirmed by SEM images of the membranes before and after ion current tests (fig. S11B). The dependence of ion selectivity of the ZIF-8/GO/AAO membrane on pH has also been studied (fig. S11C). No obvious change in Li^+/Rb^+ selectivity is observed at pH values ranging from 7 to 12, which confirms that the ZIF-8 membranes have stable Li^+/Rb^+ selectivity under basic conditions.

Moreover, ions can pass through the ZIF-8/GO/AAO membrane under very low applied voltage, down to 20 mV in our study (Fig. 2B), showing fast ion transport rates of ~10^5 ions s^{-1} for single ZIF-8/GO/AAO pores at 20 mV and ~10^6 ions s^{-1} for single ZIF-8/GO/AAO pores at 200 mV, which is comparable to the transport rate of biological ion channels (*2*, *5*). This ion transport phenomenon is very different from ion transport properties of a single ~3 Å MoS_2 pore reported by Feng *et al.* (*35*). The single MoS_2 pore could not conduct ions when the applied voltage was lower than the energy gap of the MoS_2 pore (~1200 mV for a 3 Å pore). Feng *et al.* believed that these voltage-gated ion transport properties were induced by an ionic Coulomb blockade effect. The voltage-gated properties were also found in single hydrophobic nanopores by Powell *et al.* (*36*). These studies demonstrate that the pore size is not the key factor for ionic Coulomb blockade. Furthermore, although many biological ion channels, such as biological Na^+, K^+, and Cl^- channels (*5*, *9*, *37*), have angstrom-sized ion selectivity filters, they do not exhibit any ionic Coulomb blockade effect and can conduct ions under very low voltages, down to 1 mV. Therefore, the conduction of ions at low applied voltage and high transport rates in ZIF-8/GO/AAO membranes can be attributed to the similarity of pore structures between ZIF-8 and biological ion channels.

Effects of the MOF pore size and chemistry on the alkali metal ion selectivity

To further investigate the influence of pore window diameter and chemistry on alkali metal ion selectivity of the MOF membranes, we prepared two other different MOF membranes of different pore window sizes and frameworks based on PET supports (notes S5 and S6). One is the ZIF-7/PET membrane with ~2.9 Å pore windows (smaller than ZIF-8 windows) and ~6.0 Å pore cavities, and the other is the UiO-66/PET membrane with ~6.0 Å windows (larger than ZIF-8 windows) and ~11.0 Å cavities (see Fig. 4B and fig. S12 for MOF pore window and crystal structures). The *I-V* properties of these two MOF/PET membranes with different ions are shown in fig. S13. For the ZIF-7/PET membrane, although the ZIF-7 pore has smaller window size than the ZIF-8 pore, ion conductivity and selectivity were not observed because of the superhydrophobicity of the ZIF-7 pore that is induced by the hydrophobic phenyl groups on the ZIF-7 frameworks (*15*, *22*). However, the UiO-66/PET membrane showed weak alkali metal ion selectivity because UiO-66 has a larger window diameter than the ZIF-8 pore, and less hydrophobic phenyl groups on the window framework compared with the ZIF-7 pore (Fig. 4B). A systematic comparison of the ion selectivity of the porous membranes fabricated in this study is shown in Fig. 4C and table S5, and the performance of current synthetic ion selective membranes is summarized in table S6. It is clear that the alkali metal ion selectivity of synthetic membranes decreases with increasing window diameter up to 1 nm (Fig. 4B and fig. S14). The ZIF-8/GO/AAO membranes exhibit the best selectivity of Li^+, Na^+, K^+, and Rb^+ ions relative to other synthetic membranes (table S6). Therefore, both the window size and framework chemistry play very important roles in the ion selectivity and conductivity of MOF pores.

In summary, MOF membranes with pore structures composed of subnanometer-sized windows and nanometer-sized cavities are promising candidates for separating monatomic ions of the same valence and similar sizes. The substantial alkali metal ion selectivity and conductivity observed in our experiments can be attributed to the biological ion channel–like pore morphologies of the MOF membranes. The angstrom-sized windows act as ion selectivity filters for sieving alkali metal ions, whereas the nanometer-sized cavities function as ion conductive pores

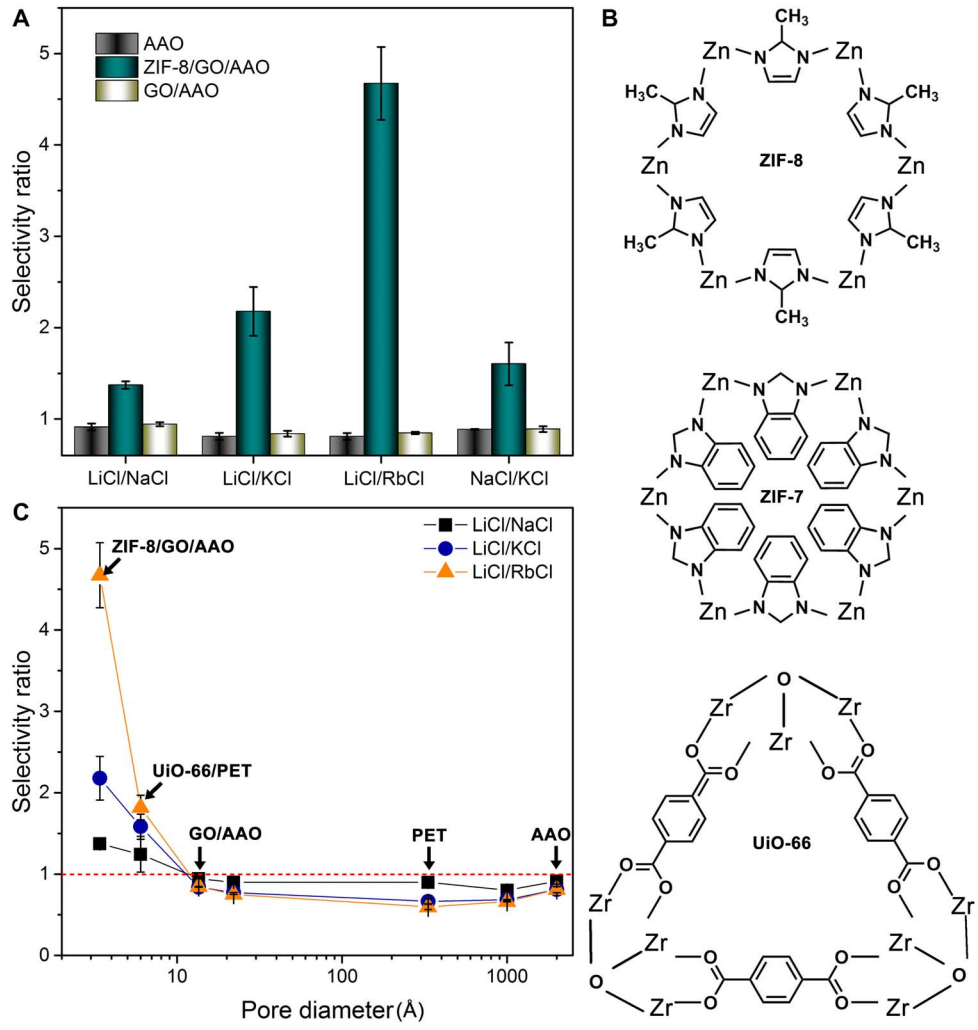

Fig. 4. Ion selectivity of synthetic MOF membranes. (**A**) Alkali metal ion selectivity of AAO supports, ZIF-8/GO/AAO membranes, and GO/AAO membranes. (**B**) Window structures of MOF pores: six-ring ZIF-8 window of ~3.4 Å in diameter, six-ring ZIF-7 window of ~2.9 Å in diameter, and triangular UiO-66 window of ~6.0 Å in diameter (see fig. S11 for crystal structures of ZIF-7 and UiO-66). (**C**) Dependence of ion selectivity on the pore widow diameter of different MOFs and the pore diameter of nanoporous membranes. At the angstrom scale, the alkali metal ion selectivity of the MOF membranes decreases with increasing window diameter. However, all membranes with pore diameters >1 nm do not have alkali metal ion selectivity.

for fast ion transport. Metal ion selectivity may be further improved by tailoring framework chemistry and pore geometry of MOF pores (*23*, *28*). Our results provide a new avenue for studying other biomimetic ion transport properties at the angstrom scale, such as rectifying and gating. Furthermore, MOF membranes may be used as platform materials to develop synthetic ion channels with high ion selectivity by chemical functionalization for a deeper understanding of ion selective transport mechanisms in subnanometer pores and for highly energy-efficient separation applications in many fields.

MATERIALS AND METHODS

Chemicals and materials

$Zn(NO_3)_2{\cdot}6H_2O$ (98.0 %), 2-methylimidazole (Hmim, 99.0%), lithium chloride (LiCl, 99.0%), sodium chloride (NaCl, 99.0%), potassium chloride (KCl, 99.0%), rubidium chloride (RbCl, 99.0%), sodium hydroxide (NaOH, 85%), hydrogen chloride (HCl, 36 to 38%), potassium hydroxide (KOH, 85%), GO, 1,4-benzenedicarboxylic acid (BDC, 98%), zirconium chloride ($ZrCl_4$, >99.5%), benzimidazole (Bim, 99.0%), and *N*,*N*′-dimethylformamide (DMF, 99.8%) were purchased from Sigma-Aldrich. Methanol (analysis) was purchased from Merck. All chemicals were used as provided. All solutions were prepared with Milli-Q water (18.2 megohm). Porous AAO disks with a diameter of 13 mm (average pore diameter of 200 nm, pore density of ~7.6×10^6 mm^{-2}) from GE Healthcare companies were used as supports.

Synthesis of hybrid ZIF-8/GO nanosheets

ZIF-8/GO nanosheets were prepared by our previously reported method (*19*). Six milliliters of methanol solution with 0.183 g of $Zn(NO_3)_2{\cdot}6H_2O$, 10 ml of methanol solution with 0.405 g of 2-methylimidazole (Hmim), and 4 ml of GO (1 mg ml^{-1}) suspension in a mixture of methanol/water (4:1, v/v) were mixed together by stirring for 3 hours, leading to the formation of ZIF-8/GO nanosheets. The molar ratio of Hmim/Zn^{2+} in this system was 8. The precipitation was collected by centrifugation (8000 rpm for 5 min) and washed with methanol three times.

Fabrication of ultrathin ZIF-8 membrane on the AAO support

Hybrid ZIF-8/GO nanosheets were redispersed in methanol to form a stable colloid suspension with a concentration of 20 mg ml^{-1}. Then, the suspension was spin-coated onto the AAO support to form ultrathin and uniform ZIF-8/GO seeding layer. The spin-coating process was performed for 30 s at 1000 rpm. After coating, the support with seeding layer was dried at 50°C for 2 hours and then coated again. Double coating was carried out to ensure formation of a uniform seeding layer on the AAO support. The coated support was dried at 50°C overnight. The ZIF-8/GO seeding layer was further etched by air plasma to make the ZIF-8/GO nanosheets nanoporous. Plasma treatment was carried out using Harrick Plasma PDC-32G-2 with 18 W of power (max) at 1-mbar pressure. Optimal time of the air plasma treatment for obtaining a nanoporous seeding layer was 30 s. The ultrathin ZIF-8/GO membrane was prepared by secondarily growing the plasma-treated seeding layer on the AAO support via the counterdiffusion method. Zn^{2+} and Hmim solutions were prepared by dissolving $Zn(NO_3)_2 \cdot 6H_2O$ (0.183 g) and Hmim (0.405 g) in 10 ml of methanol, respectively. The coated AAO support with nanoporous seeding layer was mounted on a custom-made setup, where the Zn^{2+} and Hmim solutions were separated by the coated support, the seeding layer faced the Zn^{2+} side, and the AAO support was vertically aligned. After reaction at room temperature for 3 hours, the ZIF-8/GO/AAO membranes were taken out and rinsed with fresh methanol. Last, the membranes were dried at 50°C overnight.

Characterization

SEM images were taken with field-emission scanning electron microscopes (FEI Nova NanoSEM 450 and FEI Magellan 400) operating at 5 kV. Transmission electron microscopy (TEM) images and selected area electron diffraction were taken by an FEI Tecnai G2 T20 operated at an accelerating voltage of 200 kV. Powder x-ray diffraction (PXRD) patterns were carried out in the 2θ range of 5° to 40° at room temperature using a MiniFlex600 diffractometer (Rigaku) in transmission geometry using Cu Kα radiation (15 mA and 40 kV) at a scan rate of 2° min^{-1} with a step size of 0.02°. For gas adsorption isotherms, high-purity grade (99.999%) nitrogen (N_2) was used throughout the adsorption experiments. Before the gas adsorption measurement, ZIF-8 powders were activated at 60°C for 24 hours. Low-pressure volumetric N_2 adsorption isotherms up to 1 bar were measured using a Micromeritics 3Flex gas sorption analyzer. BET surface area and pore size were determined by measuring N_2 adsorption isotherms at 77 K in a liquid nitrogen bath and calculated using the Micromeritics software.

Ion current measurement

The ion transport properties of the ZIF-8/GO/AAO membranes were studied by measuring ion currents through AAO supports before and after growth of ZIF-8/GO membranes. Ion current was measured by a Keithley 6487 picoammeter (Keithley Instruments). The membrane was mounted between two chambers of an electrochemical cell, and the test area of each membrane was ~28.26 mm^2. Ag/AgCl electrodes were used to apply a transmembrane potential across the membrane. Forward voltage was the positive potential applied on the ZIF-8/GO side of the membrane. The main transmembrane potential used in this work had been evaluated beforehand, and a scanning voltage varying from −0.2 to +0.2 V with a 40-s period was selected. The pH values of the electrolyte solutions were adjusted by 1 M NaOH, KOH, or HCl solutions. The influence of addition substance on the ionic strength of the electrolyte solutions can be ignored. Unless otherwise stated, the pH value of the electrolyte solution was 7.0. Here, each test was repeated at least three times to obtain the average current value at different voltages on the same membrane.

SUPPLEMENTARY MATERIALS

Supplementary material for this article is available at http://advances.sciencemag.org/cgi/content/full/4/2/eaaq0066/DC1

note S1. Gas permeation tests.
note S2. Fabrication of bullet-shaped single-nanochannel PET membranes.
note S3. Fabrication of single-nanochannel supported ZIF-8/PET membrane.
note S4. MD simulations.
note S5. Fabrication of single-nanochannel supported ZIF-7/PET membrane.
note S6. Fabrication of single-nanochannel supported UiO-66/PET membrane.
fig. S1. Structures of a biological ion channel and subnanometer ZIF-8 pores.
fig. S2. Fabrication process of the ZIF-8/GO/AAO membrane.
fig. S3. SEM characterization of the AAO support before and after growth of ZIF-8/GO membrane.
fig. S4. Gas permeation and selectivity of the ZIF-8/GO/AAO membrane and N_2 adsorption isotherms of ZIF-8 crystals.
fig. S5. Dependence of the ion conductance of the ZIF-8/GO/AAO membrane on the ionic diameter.
fig. S6. Ion transport properties of the nanoporous GO/AAO membrane.
fig. S7. Ion transport in the single-nanochannel supported ZIF-8/PET membrane without GO nanosheets.
fig. S8. Ion transport mechanism through subnanometer ZIF-8 pores.
fig. S9. Calculated ion velocities in ZIF-8 pores under an electric field of 0.5 V/Å.
fig. S10. Radial distribution function $g(r)$ of water molecules around Li^+ and K^+ in ZIF-8 calculated under different van der Waals forces.
fig. S11. Cycle performance and stability of the ZIF-8/GO membrane.
fig. S12. Fabrication and characterization of the ZIF-7/PET and UiO-66/PET membranes.
fig. S13. Ion transport properties of the ZIF-7/PET and UiO-66/PET membranes.
fig. S14. Ion transport properties of the multichannel PET membranes with a channel density of 10^8 cm^{-2}.
table S1. Conductance values of the AAO supports before and after growth of ZIF-8/GO membranes measured in 0.1 M MCl solutions (M^+ = Li^+, Na^+, K^+, and Rb^+).
table S2. Studied ionic species: ionic diameter (d), hydrated ionic diameter (d_H), hydration enthalpy, and limited ion conductivity.
table S3. Calculated ion mobility in bulk solution and in ZIF-8 (in unit of 10^{-7} m^2 V^{-1} s^{-1}).
table S4. Ion selectivity ratios of the three reproduced ZIF-8/GO/AAO membranes and three reproduced UiO-66/PET membranes.
table S5. Dependence of the ion selectivity on the pore diameter of the synthetic membranes.
table S6. Comparison of the ion selectivity of the ZIF-8 membranes with other synthetic membranes.
References (*38*–*50*)

REFERENCES AND NOTES

1. Y. Kim, T. T. T. Nguyen, D. G. Churchill, in *The alkali metal ions: Their Role for Life*, A. Sigel, H. Sigel, R. K. O. Sigel, Eds. (Springer International Publishing, 2016), pp. 1–10.
2. B. Hille, *Ionic Channels of Excitable Membranes* (Sinauer Associates Inc., ed. 3, 2001).
3. I. S. Joung, T. E. Cheatham, Molecular dynamics simulations of the dynamic and energetic properties of alkali and halide ions using water-model-specific ion parameters. *J. Phys. Chem. B* **113**, 13279–13290 (2009).
4. J. Payandeh, T. Scheuer, N. Zheng, W. A. Catterall, The crystal structure of a voltage-gated sodium channel. *Nature* **475**, 353–358 (2011).
5. X. Zhang, W. Ren, P. DeCaen, C. Yan, X. Tao, L. Tang, J. Wang, K. Hasegawa, T. Kumasaka, J. He, J. Wang, D. E. Clapham, N. Yan, Crystal structure of an orthologue of the nachbac voltage-gated sodium channel. *Nature* **486**, 130–134 (2012).
6. G. M. Lipkind, H. A. Fozzard, Voltage-gated na channel selectivity: The role of the conserved domain III lysine residue. *J. Gen. Physiol.* **131**, 523–529 (2008).
7. H. Zhang, Y. Tian, L. Jiang, Fundamental studies and practical applications of bio-inspired smart solid-state nanopores and nanochannels. *Nano Today* **11**, 61–81 (2016).
8. T. Sata, Modification of transport properties of ion exchange membranes, in *Ion exchange membranes: Preparation, characterization, modification and application*, T. Sata, Ed. (The Royal Society of Chemistry, 2004), pp. 135–214.
9. D. A. Doyle, J. M. Cabral, R. A. Pfuetzner, A. Kuo, J. M. Gulbis, S. L. Cohen, B. T. Chait, R. MacKinnon, The structure of the potassium channel: Molecular basis of K^+ conduction and selectivity. *Science* **280**, 69–77 (1998).

10. P. Sun, K. Wang, H. Zhu, Recent developments in graphene-based membranes: Structure, mass-transport mechanism and potential applications. *Adv. Mater.* **28**, 2287–2310 (2016).
11. K. B. Jirage, J. C. Hulteen, C. R. Martin, Nanotubule-based molecular-filtration membranes. *Science* **278**, 655–658 (1997).
12. R. K. Joshi, P. Carbone, F. C. Wang, V. G. Kravets, Y. Su, I. V. Grigorieva, H. A. Wu, A. K. Geim, R. R. Nair, Precise and ultrafast molecular sieving through graphene oxide membranes. *Science* **343**, 752–754 (2014).
13. P. K. Choubey, M.-s. Kim, R. R. Srivastava, J.-c. Lee, J.-Y. Lee, Advance review on the exploitation of the prominent energy-storage element: Lithium. Part I: From mineral and brine resources. *Miner. Eng.* **89**, 119–137 (2016).
14. N. Stock, S. Biswas, Synthesis of metal-organic frameworks (mofs): Routes to various mof topologies, morphologies, and composites. *Chem. Rev.* **112**, 933–969 (2012).
15. J. Yao, H. Wang, Zeolitic imidazolate framework composite membranes and thin films: Synthesis and applications. *Chem. Soc. Rev.* **43**, 4470–4493 (2014).
16. B. Seoane, J. Coronas, I. Gascon, M. E. Benavides, O. Karvan, J. Caro, F. Kapteijn, J. Gascon, Metal–organic framework based mixed matrix membranes: A solution for highly efficient CO_2 capture? *Chem. Soc. Rev.* **44**, 2421–2454 (2015).
17. H. Guo, G. Zhu, I. J. Hewitt, S. Qiu, "Twin copper source" growth of metal–organic framework membrane: $Cu_3(BTC)_2$ with high permeability and selectivity for recycling H_2. *J. Am. Chem. Soc.* **131**, 1646–1647 (2009).
18. Y. S. Li, H. Bux, A. Feldhoff, G.-L. Li, W.-S. Yang, J. Caro, Controllable synthesis of metal–organic frameworks: From MOF nanorods to oriented MOF membranes. *Adv. Mater.* **22**, 3322–3326 (2010).
19. Y. Hu, J. Wei, Y. Liang, H. Zhang, X. Zhang, W. Shen, H. Wang, Zeolitic imidazolate framework/graphene oxide hybrid nanosheets as seeds for the growth of ultrathin molecular sieving membranes. *Angew. Chem. Int. Ed.* **55**, 2048–2052 (2016).
20. Z. Chen, W. Zhang, C.-A. Palma, A. L. Rizzini, B. Liu, A. Abbas, N. Richter, L. Martini, X.-Y. Wang, N. Cavani, H. Lu, N. Mishra, C. Coletti, R. Berger, F. Klappenberger, M. Kläui, A. Candini, M. Affronte, C. Zhou, V. De Renzi, U. del Pennino, J. V. Barth, H. J. Räder, A. Narita, X. Feng, K. Müllen, Synthesis of graphene nanoribbons by ambient-pressure chemical vapor deposition and device integration. *J. Am. Chem. Soc.* **138**, 15488–15496 (2016).
21. Y. Peng, Y. Li, Y. Ban, H. Jin, W. Jiao, X. Liu, W. Yang, Metal-organic framework nanosheets as building blocks for molecular sieving membranes. *Science* **346**, 1356–1359 (2014).
22. A. Phan, C. J. Doonan, F. J. Uribe-Romo, C. B. Knobler, M. O'Keeffe, O. M. Yaghi, Synthesis, structure, and carbon dioxide capture properties of zeolitic imidazolate frameworks. *Acc. Chem. Res.* **43**, 58–67 (2010).
23. M. S. Denny Jr., J. C. Moreton, L. Benz, S. M. Cohen, Metal–organic frameworks for membrane-based separations. *Nat. Rev. Mater.* **1**, 16078 (2016).
24. X. Liu, X. Liu, H. Jin, Y. Li, H. Bux, Z. Hu, Y. Ban, W. Yang, Metal–organic framework ZIF-8 nanocomposite membrane for efficient recovery of furfural via pervaporation and vapor permeation. *J. Membr. Sci.* **428**, 498–506 (2013).
25. X. L. Liu, Y.-S. Li, G.-Q. Zhu, Y.-J. Ban, L.-Y. Xu, W.-S. Yang, An organophilic pervaporation membrane derived from metal–organic framework nanoparticles for efficient recovery of bio-alcohols. *Angew. Chem. Int. Ed.* **50**, 10636–10639 (2011).
26. Y. Hu, X. Dong, J. Nan, W. Jin, X. Ren, N. Xua, Y. M. Lee, Metal–organic framework membranes fabricated via reactive seeding. *Chem. Commun.* **47**, 737–739 (2011).
27. A. Sotto, G. Orcajo, J. M. Arsuaga, G. Calleja, J. Landaburu-Aguirre, Preparation and characterization of MOF-PES ultrafiltration membranes. *J. Appl. Polym. Sci.* **132**, 41633 (2015).
28. C. Wang, X. Liu, N. Keser Demir, J. P. Chen, K. Li, Applications of water stable metal–organic frameworks. *Chem. Soc. Rev.* **45**, 5107–5134 (2016).
29. X. Liu, N. K. Demir, Z. Wu, K. Li, Highly water-stable zirconium metal–organic framework uio-66 membranes supported on alumina hollow fibers for desalination. *J. Am. Chem. Soc.* **137**, 6999–7002 (2015).
30. Z. Hu, Y. Chen, J. Jiang, Zeolitic imidazolate framework-8 as a reverse osmosis membrane for water desalination: Insight from molecular simulation. *J. Chem. Phys.* **134**, 134705 (2011).
31. K. M. Gupta, Z. Qiao, K. Zhang, J. Jiang, Seawater pervaporation through zeolitic imidazolate framework membranes: Atomistic simulation study. *ACS Appl. Mater. Interfaces* **8**, 13392–13399 (2016).
32. A. J. Brown, N. A. Brunelli, K. Eum, F. Rashidi, J. R. Johnson, W. J. Koros, C. W. Jones, S. Nair, Interfacial microfluidic processing of metal-organic framework hollow fiber membranes. *Science* **345**, 72–75 (2014).
33. E. R. Nightingale Jr., Phenomenological theory of ion solvation. Effective radii of hydrated ions. *J. Phys. Chem.* **63**, 1381–1387 (1959).
34. A. F. P. Ferreira, M. C. Mittelmeijer-Hazeleger, M. A. Granato, V. F. Duarte Martins, A. E. Rodrigues, Gadi Rothenberg, Sieving di-branched from mono-branched and linear alkanes using ZIF-8: Experimental proof and theoretical explanation. *Phys. Chem. Chem. Phys.* **15**, 8795–8804 (2013).
35. J. Feng, K. Liu, M. Graf, D. Dumcenco, A. Kis, M. D. Ventra, A. Radenovic, Observation of ionic coulomb blockade in nanopores. *Nat. Mater.* **15**, 850–855 (2016).
36. M. R. Powell, L. Cleary, M. Davenport, K. J. Shea, Z. S. Siwy, Electric-field-induced wetting and dewetting in single hydrophobic nanopores. *Nat. Nanotechnol.* **6**, 798–802 (2011).
37. R. Dutzler, E. B. Campbell, M. Cadene, B. T. Chait, R. MacKinnon, X-ray structure of a clc chloride channel at 3.0Å reveals the molecular basis of anion selectivity. *Nature* **415**, 287–294 (2002).
38. J. Wang, R. Fang, J. Hou, H. Zhang, Y. Tian, H. Wang, L. Jiang, An oscillatory reaction induced periodic C-quadruplex DNA gating of artificial ion channels. *ACS Nano* **11**, 3022–3029 (2017).
39. L. Zhang, Z. Hu, J. Jiang, Sorption-induced structural transition of zeolitic imidazolate framework-8: A hybrid molecular simulation study. *J. Am. Chem. Soc.* **135**, 3722–3728 (2013).
40. N. Foloppe, A. D. MacKerell Jr., All-atom empirical force field for nucleic acids: I. Parameter optimization based on small molecule and condensed phase macromolecular target data. *J. Comput. Chem.* **21**, 86–104 (2000).
41. W. L. Jorgensen, D. S. Maxwell, J. Tirado-Rives, Development and testing of the opls all-atom force field on conformational energetics and properties of organic liquids. *J. Am. Chem. Soc.* **118**, 11225–11236 (1996).
42. W. L. Jorgensen, J. Tirado-Rives, The OPLS [optimized potentials for liquid simulations] potential functions for proteins, energy minimizations for crystals of cyclic peptides and crambin. *J. Am. Chem. Soc.* **110**, 1657–1666 (1988).
43. S. Koneshan, J. C. Rasaiah, R. M. Lynden-Bell, S. H. Lee, Solvent structure, dynamics, and ion mobility in aqueous solutions at 25°C. *J. Phys. Chem. B* **102**, 4193–4204 (1998).
44. Y. Ying, Y. Xiao, J. Ma, X. Guo, H. Huang, Q. Yang, D. Liua, C. Zhong, Recovery of acetone from aqueous solution by ZIF-7/PDMS mixed matrix membranes. *RSC Adv.* **5**, 28394–28400 (2015).
45. D. W. Smith, Ionic hydration enthalpies. *J. Chem. Educ.* **54**, 540 (1977).
46. A. W. Adamson, Textbook of Physical Chemistry (Academic Press, ed. 1, 1973), pp. 512.
47. Q. Wen, D. Yan, F. Liu, M. Wang, Y. Ling, P. Wang, P. Kluth, D. Schauries, C. Trautmann, P. Apel, W. Guo, G. Xiao, J. Liu, J. Xue, Y. Wang, Highly selective ionic transport through subnanometer pores in polymer films. *Adv. Funct. Mater.* **26**, 5796–5803 (2016).
48. J. Abraham, K. S. Vasu, C. D. Williams, K. Gopinadhan, Y. Su, C. T. Cherian, J. Dix, E. Prestat, S. J. Haigh, I. V. Grigorieva, P. Carbone, A. K. Geim, R. R. Nair, Tunable sieving of ions using graphene oxide membranes. *Nat. Nanotechnol.* **12**, 546–550 (2017).
49. R. H. Tunuguntla, R. Y. Henley, Y.-C. Yao, T. A. Pham, M. Wanunu, A. Noy, Enhanced water permeability and tunable ion selectivity in subnanometer carbon nanotube porins. *Science* **357**, 792–796 (2017).
50. W. Choi, Z. W. Ulissi, S. F. E. Shimizu, D. O. Bellisario, M. D. Ellison, M. S. Strano, Diameter-dependent ion transport through the interior of isolated single-walled carbon nanotubes. *Nat. Commun.* **4**, 2397 (2013).

Acknowledgments: We would like to thank Y. Li and J. Lu for their help with the N_2 adsorption and desorption experiments. We also thank the staff of Monash Centre for Electron Microscopy at Monash University for their technical assistance with the SEM. **Funding:** This research is supported by the Australian Research Council (DP150100765, DP180100298, and DE170100006). The work of B.D.F. was supported by the Australian-American Fulbright Commission for the award to B.D.F. of the U.S. Fulbright Distinguished Chair in Science, Technology and Innovation sponsored by the Commonwealth Scientific and Industrial Research Organization. The MD simulation was undertaken with the assistance of resources and services from the National Computational Infrastructure, which is supported by the Australian Government.
Author contributions: H.Z. and H.W. designed the project. H.Z., J.H., Y.H., and R.O. performed the sample preparations, electrochemical measurements, gas separations, and TEM, SEM, and XRD characterizations. J.Z.L. and P.W. performed the computational study of MD simulations. H.Z., J.Z.L., L.J., B.D.F., A.J.H., and H.W. analyzed the results and co-wrote the paper. **Competing interests:** H.Z., H.W., B.D.F., and A.J.H. are inventors on a provisional patent application related to this work submitted by Monash University (serial no. AU2017905029, filed 05 Dec 2017). The authors declare that they have no other competing interests. **Data and materials availability:** All data needed to evaluate the conclusions in the paper are present in the paper and/or the Supplementary Materials. Additional data related to this paper may be requested from the authors.

Submitted 23 September 2017
Accepted 11 January 2018
Published 9 February 2018
10.1126/sciadv.aaq0066

Citation: H. Zhang, J. Hou, Y. Hu, P. Wang, R. Ou, L. Jiang, J. Z. Liu, B. D. Freeman, A. J. Hill, H. Wang, Ultrafast selective transport of alkali metal ions in metal organic frameworks with subnanometer pores. *Sci. Adv.* **4**, eaaq0066 (2018).

Ultrafast selective transport of alkali metal ions in metal organic frameworks with subnanometer pores

Huacheng Zhang, Jue Hou, Yaoxin Hu, Peiyao Wang, Ranwen Ou, Lei Jiang, Jefferson Zhe Liu, Benny D. Freeman, Anita J. Hill and Huanting Wang

Sci Adv **4** (2), eaaq0066.
DOI: 10.1126/sciadv.aaq0066